Received: 27 June 2022 | Revised: 5 November 2022 | Accepted: 4 January 2023

DOI: 10.1111/jace.19010

Journal of the American Ceramic Society

SPECIAL ISSUE ARTICLE

Growth of titania and tin oxide from Ti_2SnC via rapid thermal oxidation in air for lithium-ion battery application

Shae Jolly[1] | **Samantha Husmann**[2] | **Volker Presser**[2,3,4] | **Michael Naguib**[1]

[1]Department of Physics and Engineering Physics, Tulane University, New Orleans, Louisiana, USA

[2]INM, – Leibniz Institute for New Materials, Saarbrücken, Germany

[3]Department of Materials Science and Engineering, Saarland University, Saarbrücken, Germany

[4]Saarene – Saarland Center for Energy Materials and Sustainability, Saarbrücken, Germany

Correspondence
Volker Presser, INM – Leibniz Institute for New Materials, D2 2, 66123 Saarbrücken, Germany.
Email: volker.presser@leibniz-inm.de

Michael Naguib, Department of Physics and Engineering Physics, Tulane University, New Orleans, LA 70118, USA.
Email: naguib@tulane.edu

Funding information
Fluid Interface Reactions, Structures, and Transport (FIRST) Center, an Energy Frontier Research Center (EFRC) funded by the U.S. Department of Energy (DOE), Office of Science, Office of Basic Energy Sciences; The German Research Foundation (DFG, Deutsche Forschungsgemeinschaft), Grant/Award Number: PR-1173/9

Abstract

Herein, we report the synthesis of TiO_2–SnO_2–C/carbide hybrid electrode materials for Li-ion batteries (LIBs) via two different methods of controlled oxidation of layered Ti_2SnC. The material was partially oxidized in an open-air furnace (OAF) or using a rapid thermal annealing (RTA) approach to obtain the desired TiO_2–SnO_2–C/carbide hybrid material; the carbide phase encompassed both residual Ti_2SnC and TiC as a reaction product. We tested the oxidized materials as an anode in a half cell to investigate their electrochemical performance in LIBs. Analysis of the various oxidation conditions indicated the highest initial lithiation capacity of 838 mAh/g at 100 mA/g for the sample oxidized in the OAF at 700°C for 1 h. Still, the delithiation capacity dropped to 427 mAh/g and faded over cycling. Long-term cycling demonstrated that the RTA sample treated at 800°C for 30 s was the most efficient, as it demonstrated a reversible capacity of around 270 mAh/g after 150 cycles, as well as a specific capacity of about 150 mAh/g under high cycling rate (2000 mA/g). Given the materials' promising performance, this processing method could likely be applied to many other members of the MAX family, with a wide range of energy storage applications.

KEYWORDS
energy storage, MAX phase, metal oxide, tin oxide

1 | INTRODUCTION

Lithium-ion batteries (LIBs) have become the most widely used electrochemical energy storage devices due to their high energy density, long cycling lives, temperature independence, and low self-discharge rates.[1] As the research community explores materials based on abundance, environmental impact, and safety, transition metal oxides have emerged as a promising choice for LIB anodes. These metal oxides are simple to synthesize and have low production costs while demonstrating remarkable electrochemical stability.[2,3] Usage of nanostructures, such as nanotubes

and nanowires, of these transition metal oxides can further improve their performance in LIBs.[4] For example, titania nanotube arrays have demonstrated high capacity retention and improved durability of LIBs.[5]

Titanium dioxide (TiO_2) is an attractive LIB anode material due to its safe operation potential and limited volume change with lithium insertion and de-insertion. However, its relatively low electric conductivity and low specific capacity limit its use.[6–8] When utilized as an anode material, TiO_2 exhibits a capacity well below its theoretical capacity of 335 mAh/g due to its low conductivity and slow insertion rates.[9–13] The insertion of lithium is a diffusion-controlled process,[14,15] so modifying the TiO_2 morphology can aid in the demonstrated capacities.[16,17] Further, SnO_2 has gathered attention as an anode material due to the high theoretical capacity of $Li_{4.4}Sn$ (944 mAh/g).[18] Yet, the large volume expansion associated with lithium insertion in tin[19] leads to stress on the anode, limiting the long-term cycling stability associated with the material.[20,21] Due to these limitations of TiO_2 and SnO_2, both are utilized as components of composite anode material, typically alongside graphene.[22–25]

MAX phases are a group of hexagonal, layered carbides/nitrides of the formula $M_{n+1}AX_n$, where M is an early transition metal, A is a group 13 or 14 element, X is carbon and/or nitrogen, and $n = 1–4$.[26] Acid etching of MAX phases results in their two-dimensional derivative MXenes ($M_{n+1}X_nT_x$; where T_x stands for different surface terminations).[27] Due to their high electrical and low diffusion barrier of Li on their surfaces,[28] MXenes have demonstrated a promising performance as electrode material in LIBs, especially at high cycling rates.[29,30] To improve the cycle life and increase the capacity of MXene electrodes, controlled oxidation of the multilayer MXene has been studied as a processing method. For example, heating $Ti_3C_2T_x$ MXene in air leads to TiO_2 nanocrystals enmeshed in graphitic carbon sheets, allowing extremely high cycling rates in LIBs.[31] Zhao et al. also demonstrated that various other methods, including alternating filtration, in situ wet chemistry, and spray coating, can form hybrid materials of $Ti_3C_2T_x$ MXene and TMOs like Co_3O_4 and $NiCo_2O_4$ for LIB anodes.[32] MXenes can be considered the building blocks for MAX phases, and these building blocks are bonded through A metal layers (e.g., Al, Sn, Ga, and Ge). The successful synthesis of TMO-MXene or TMO-carbon hybrids by controlled oxidation of MXene indicates that hybrids coexisting with A metal oxide (i.e., A_yO_z) could be derived directly from MAX phases without a hazardous etching process to synthesize MXene from the MAX phase before oxidation.

Many elements constituting A layers in MAX phases, like Sn, have high specific capacities for Li. However, when tested as anode material, the Sn in Nb_2SnC does not deliver the theoretical capacity of Sn, although Zhao et al. found that the capacity nearly doubles (from 87 to 150 mAh/g) over the cycling period.[33] The increase in capacity was also found in a study on V_2SnC (from about 100 to about 300 mAh/g over the course of 900 cycles at 1 A/g).[34] The lack of changes in the structure of both Nb_2SnC and V_2SnC upon lithiation and del-lithiation suggests that the Li storage is limited to the surface of the MAX phases.[34] Electrochemical oxidation of MAX phases exposes a larger surface area to lithium with partial oxidation of M and/or A components, allowing for the creation of hybrid materials of oxides and carbides. For example, the anodization of Ti_3SiC_2 with HF electrolyte results in titania, silica, and carbide hybrid with high performance as a negative electrode in thin-film LIBs.[35] Combining these oxidation methods with a tin-containing MAX phase could help harness more capacity from tin than is accessible in as-synthesized $M_{n+1}SnC_n$. Carbides can be attractive precursors for the synthesis of oxides with unique morphology, hybridization, and/or structure.[36,37]

Studying the oxidation behavior of $Ti_2Al_{1-x}Sn_xC$ and Ti_2SnC versus Ti_2AlC has indicated that adding Sn leads to accelerated oxidation of the MAX phase.[38,39] Dong et al. observed minimal oxidation resistance of Ti_2SnC in air.[40] The latter work identified an oxidation/decomposition/oxidation system where below 500°C, oxidation of Ti_2SnC was the primary reaction, whereas, above 500°C, the decomposition of Ti_2SnC followed by oxidation of TiC_x and Sn governed.[40] Zhou et al. later studied the isothermal oxidation behaviors of Ti_2SnC from 500 to 800°C and found that it is led by the inward diffusion of oxygen and outward diffusion of titanium. At the same time, tin stays relatively static within the matrix, thus explaining the observed presence of unreacted metallic tin in the formed composite material.[38] This suggests that mild oxidation conditions might be sufficient to form a hybrid structure of transition metal oxide, tin oxide with carbide, and/or carbon. However, the impact of oxidation of the Sn-containing MAX phase on its electrochemical performance regarding LIBs has not been investigated. Based on the combined success of oxidation of MAX phases (and their MXene counterparts), the high theoretical capacity of tin, and the electrochemical properties of SnO_2 and TiO_2, we hypothesize that the controlled oxidation of Ti_2SnC would produce an interesting anode material for LIBs. The present study explored the MAX phase as a precursor for electrochemically viable hybrids of metal oxides and conductive carbon/carbide. In addition to electrochemical testing, X-ray diffraction (XRD), scanning and transmission electron microscopes (TEM), as well as Raman spectroscopy were utilized to investigate the oxidation products of Ti_2SnC in air.

2 | EXPERIMENTAL SECTION

2.1 | MAX phase synthesis and characterization

To synthesize the initial Ti_2SnC MAX phase, powders of titanium (≥99.5% purity, <45 μm size, Alfa Aesar), tin (≥99.85% purity, <150 μm size, Alfa Aesar), and graphite (≥99% purity, 7–11 μm size, Alfa Aesar) were combined in the molar ratio of 2:1:1 and then mixed with yttria-stabilized zirconia balls in a Turbula powder mixer for 3 h at 46 rpm. This powder mixture was then transferred to an alumina crucible, placed in a Sentrotech tube furnace under flowing argon, and heated at 10°C/min to 1250°C. The temperature was held for 2 h, and then the system was allowed to cool to room temperature. The sintered material was ground via mortar and pestle to particle sizes under 45 μm.

We used XRD to characterize the obtained powders. Our results indicated successful Ti_2SnC formation, along with some unreacted tin. To remove the unreacted tin, 10 g of the furnaced powder was stirred in 100 mL of 10% HCl (37%, Fisher Scientific) solution for 24 h at room temperature. Following this acid treatment, the powder was washed using deionized water to a pH of 7 and then dried onto filter paper via vacuum-assisted filtration. XRD confirmed the successful removal of all elemental tin from the material. Following the synthesis of the pure Ti_2SnC, these samples were oxidized in a controlled manner via open-air furnace (OAF) heating or rapid thermal annealing (RTA).

2.2 | Open-air furnace (OAF) treatment

After the successful synthesis of Ti_2SnC, powder aliquots of 0.5 g were placed into alumina crucibles and heated in a box furnace under ambient oxygen. The samples were heated at 10°C/min to various temperatures (500, 600, and 700°C) and held for 1 or 2 h before cooling to room temperature.

2.3 | Rapid thermal annealing (RTA)

For this oxidation mechanism, 0.3 g of the Ti_2SnC powders were evenly spread onto a silicon wafer and then loaded into an AG Heatpulse 610 Rapid Thermal Annealer under an open atmosphere. The system heated within 30 s until the set temperature was reached, and then the set temperature was held for a specified time before rapidly cooling to room temperature. All synthesis parameters (set temperature and holding times) are provided in Table 1.

2.4 | Material analysis and electrochemical testing

The MAX phase-containing powders were analyzed at each step with a copper K_α powder XRD (Rigaku D/MAX-2000) from 2θ of 3°–80° with a 0.02 step and recording rate of 1°/min. Phase analysis was done with DIFFRAC.EVA (Bruker AXS) and qualitative Rieveld refinement by HKL fits of the matching phases using the software TOPAS 6 from Bru. The MAX oxidation was studied by thermogravimetric analysis (TGA) (Netzsch TG 209 F1 Libra system) by heating up to 1000°C at 10°C/min under CO_2 or synthetic air atmosphere (20 mL/min) and holding temperature for 1 h.

Raman spectroscopy was performed to characterize further the composition of the oxidized Ti_2SnC powders using a Renishaw InVia microscope with an objective lens of a numeric aperture of 0.75 and an excitation wavelength of 532 nm at 0.5 mW power on the sample. The spectra were acquired with 20 s grating time for 3 accumulations at each point, with a minimum of 10 spectra collected for each sample. The depicted spectra are representative of the samples. An Si standard was used for spectral calibration before the measurements.

Scanning electron microscopy (SEM) and TEM images were taken to visualize the microstructure of the oxidized powders. SEM was carried out with a ZEISS Gemini 500 microscope with 0.5 kV acceleration voltage and an in-lens secondary electron detector. The powder samples were directly mounted to an aluminum stub with a Cu double-sided tape, and no conductive sputtering was used. TEM images were acquired with a 2100F JEOL microscope at an acceleration voltage of 200 kV. The samples were dispersed in ethanol and drop cast on copper grids coated with lacey carbon.

We studied the obtained oxidized material as a lithium-ion battery electrode. To this end, we prepared half-cell coin cells (CR2032). The working electrode was composed of the oxidized material with added conductive carbon black (acetylene black, >99.9%, Alfa Aesar) and the polymer binder polyvinylidene difluoride (PVDF, EQ-Lib-PVDF, MTI Corp.) in a mass ratio of 8:1:1. These components were vigorously mixed in a mortar and pestle until fully homogenous. *N*-methyl-2-pyrrolidone of 1 mL was added while continuously mixing until a smooth slurry was formed. The slurries were then drop-casted onto copper foil at approximate loading of ~1 mg/cm^2 and allowed to dry at 80°C, before being moved into a glove box of inert argon atmosphere (O_2 and H_2O levels <1 ppm).

The working electrodes were placed in a coin-cell case; a glass microfiber (GF/D, Whatman) separator was placed and saturated with an electrolyte of 1 M lithium

TABLE 1 Thermal treatment conditions for rapid treatment annealing.

Set temperature	500°C		600°C		700°C		800°C		1000°C		
Holding time (min:s)	5:00	10:00	5:00	10:00	5:00	10:00	0:30	2:00	5:00	0:30	5:00

hexafluorophosphate ($LiPF_6$) in ethylene carbonate (EC) and ethyl methyl carbonate (EMC) solvents with a ratio of EC:EMC = 3:7 (LP 57, Gotion). A cleaned lithium foil was then placed on the saturated separator, followed by a spacer and wave spring. The coin-cell case was then placed into an automated crimping machine to seal them. The cells were removed from the glove box and immediately loaded into a temperature-controlled chamber for electrochemical testing at 30°C. Specific capacity and cycling measurements were gathered using LANHE LAND Battery Testing System CT2001A, whereas cyclic voltammetry at 0.1 mV/s and electrochemical impedance spectroscopy (EIS) at the open-circuit voltage at frequencies between 200 kHz and 10 mHz were gathered via BioLogic VMP3 potentiostat. All potential values reported here are versus Li/Li^+ because Li was used as a counter/reference electrode.

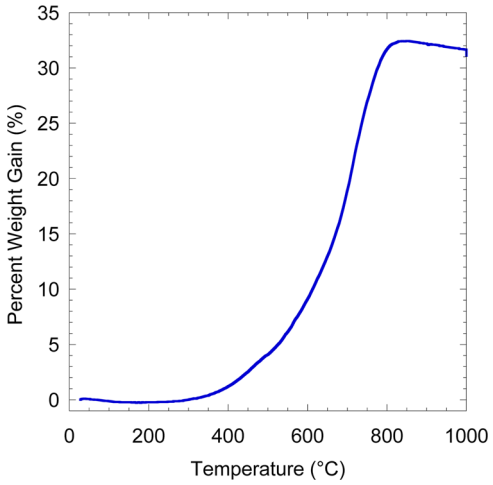

FIGURE 1 Thermogravimetric analysis (TGA) of Ti_2SnC under synthetic air atmosphere (20 mL/min) acquired at a heating rate of 10°C/min.

3 | RESULTS AND DISCUSSION

3.1 | Material characterization

The starting material for our battery-material synthesis was Ti_2SnC, which we obtained by thermal processing. The initial XRD of the synthesized MAX powder after heating the elemental precursors at 1250°C under Ar indicated the successful formation of Ti_2SnC (PDF 01-085-6647), along with a small TiC impurity, and unreacted Sn (Figure S1). An XRD pattern of the product after etching indicated the successful removal of the unreacted Sn without affecting Ti_2SnC (Figure S1). TGA was performed to observe the oxidation behavior of the material (Supporting Information, Figure 1). The oxidation of the MAX phase slowly starts at 320°C. Pronounced oxidation occurs within the temperature range of 400–836°C, with a maximum slope at 714°C. The oxidation of Ti and Sn leads to a total mass gain of 33%, close to the theoretical mass gain for a full conversion of Ti_2SnC into TiO_2 and SnO_2 (37%). This curve shows that a temperature above 800°C in air yields a completely oxidized MAX phase. A similar trend is expected for the OAF thermal treatments because heating was carried out at the same rate as the one that was used for TGA. RTA in air with short holding times (30 s to 10 min) at any temperature may deviate from the TGA-predicted outcomes due to diffusion kinetic limitations. Our results indicated that partial oxidation of the initial Ti_2SnC MAX phase was achieved even at 1000°C when the high heating rate and short holding time (only 30 s at 1000°C) of RTA treatments are employed. Our study label samples according to temperature, time, and oxidation method (e.g., 700-1hOAF refers to Ti_2SnC oxidized via OAF treatment at 700°C for 1 h).

Following the oxidation of the Ti_2SnC powders, XRDs were obtained (Figure 2A,B). The analysis of the XRDs indicates the gradual reduction in the MAX phase and appearance of TiO_2 and SnO_2 with increasing heating temperature and time. For a further qualitative assessment of the phases present in each sample, the patterns were analyzed by Rietveld refinement. The phases present in each sample are displayed in Figure 2C. The fittings of 800-30sRTA with the present phases and estimation of average composition are presented in Figure S2. The fitting of all samples is seen in Figure S3. The values of mass% are to be understood in a semiquantitative context because the preferential orientation of the layered MAX phase leads to overestimating and underestimating certain phases and an overall inaccuracy in the fitting, as observed from the high residual factor of sample 500-2hOAF composed solely of Ti_2SnC.

The OAF samples show no evidence of Ti_2SnC oxidation with heating to 500°C for 1 or 2 h, but a change in the XRD indicates the beginning of oxidation at 600°C for 1 h. At this condition, new oxide peaks begin to appear at the cost of reducing the Ti_2SnC (002) diffraction peak intensity. Ti_2SnC and metallic tin are present together with the mixture of TiO_2 and SnO_2. Prolonged oxidation times at

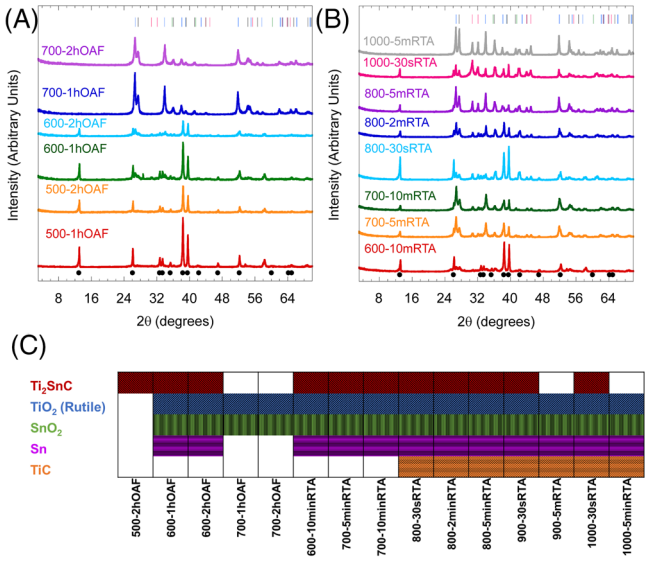

FIGURE 2 X-ray diffractograms of Ti_2SnC after oxidation via open-air furnacing (OAF) (A) and rapid thermal annealing (RTA) (B). The circle marker represents the peaks position of Ti_2SnC (PDF 01-085-6647), the black dash for TiO_2 (PDF 01-079-5860), the green dash for TiC (PDF 01-070-7697), the pink dash for Sn (PDF 01-085-4244), and the blue dash for SnO_2 (PDF 01-075-9494). Phases identified in the Ti_2SnC MAX phase oxidized at different conditions obtained by Rietveld refinement of the X-ray diffractograms (C).

600°C led to the further decomposition of the MAX phase and the gradual increase of both oxides. The increase of the oxidation peak intensity and decrease of the Ti_2SnC peaks continues until temperatures at or above 700°C, at which there is the complete removal of Ti_2SnC and total oxidation is achieved, producing a sample composed of approximately 67 mass% rutile and 33 mass% SnO_2. The RTA samples show a relative increase in oxidation peaks and a decrease in Ti_2SnC peaks from 600°C 10 min to 800°C 30 s. Longer holding times display a higher peak intensity ratio of oxide to Ti_2SnC than lower holding times at the same temperature. The (002) Ti_2SnC peak only fully disappears after treatment at 1000°C for 5 min. Nevertheless, the RTA oxidation leads to more complex compositions. At lower temperatures of 600 and 700°C, the samples are mainly composed of rutile and SnO_2. Compared to the OAF treatment, the reduced treatment time of RTA (30 s of heating and a maximum of 10 min of holding time) causes oxygen depletion. Thus, no complete oxidation is achieved, and residual Ti_2SnC and metallic Sn are present.

At 800°C and above, TiC emerges as a significant phase in the samples' composition. The mechanism of Ti_2SnC oxidation occurs through an oxidation–decomposition–oxidation process, according to the following equations:[40]

$$Ti_2SnC + 4O_2 \rightarrow SnO_2 + 2TiO_2 + CO_2 \quad (1)$$

$$Ti_2SnC \rightarrow Sn + 2TiC_{0.5} \quad (2)$$

$$TiC_{0.5} + 1.5O_2 \rightarrow TiO_2 + 0.5CO_2 \quad (3)$$

$$Sn + O_2 \rightarrow SnO_2 \quad (4)$$

According to Equation (1), the reaction occurs at lower temperatures. The decomposition of Ti_2SnC (Equation 2) and the following oxidation reactions according to Equations (3) and (4) take place at higher temperatures. This system's threshold between oxidation and decomposition of Ti_2SnC seems to occur at 800°C. This is higher than what has often been reported for this system (500–600°C).[40,41] This upshift in the threshold temperature is due mainly to the reduced oxygen content and exposure time to the MAX phase.

When the treatment times are increased from 30 s to 2 or 5 min, there is a decrease in the amount of TiC (from >35 mass% at 30 s to <15 mass% at 5 min), followed by an increase in the oxide content. The effect of the temperature can be observed by a pronounced decomposition (in 30 s) with the increase in TiC and Sn contents, and oxidation (in 5 min) with consumption of these phases and increase of oxides content from 800 to 900 and 1000°C. Even though tin is known to oxidize already at 150°C, metallic Sn is present even at higher temperatures or prolonged times. Cross-sectional analysis of bulk oxidized Ti_2SnC samples indicates that Sn-rich regions are formed at the interface between Ti_2SnC and TiO_2/SnO_2, trapped and protected from oxidation.[38] In general, there is a higher content of SnO_2 in the samples oxidized at lower temperatures. This is because reaction (1), taking place at lower temperatures, is driven by the oxidation of Sn, which has a weaker bond to Ti_6C octahedra. With the increase in temperature, an increase in the diffusion of Ti and C, and the Sn interlayer leads to a swap in the oxidation process that favors Ti rather than Sn.[38,39] It is worth noting that, according to the Ellingham diagram, the oxidation reaction of Ti is thermodynamically more favorable than that of Sn. Thus, in the presence of limited O_2 content diffused in the material, TiO_2 is preferentially formed first.

In addition to XRD, we also carried out Raman spectroscopy. The recorded Raman spectra (Figure 3A,B) further illustrate the gradual oxidation and decomposition of the MAX phase. After thermal treatments, the spectral region between 1200 and 1700 cm^{-1} features signals related to carbon vibrational modes. The band at ca. 1350 cm^{-1} is the D-band and is assigned disordered carbon. The band at ca. 1600 cm^{-1} is the G-band and relates to sp^2-hybridization carbon. Upon the heat treatment and oxidation of the metal species, these bands start to arise due to the formation of free carbon. For the OAF process,

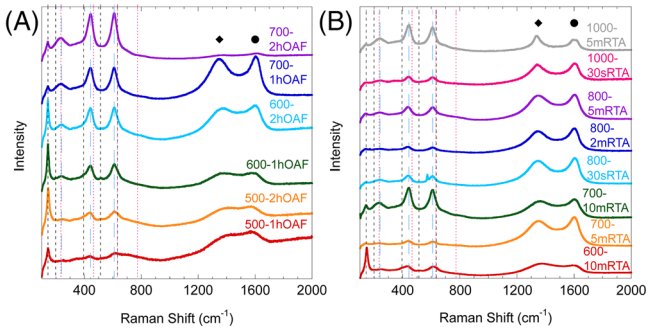

FIGURE 3 Raman spectra of Ti_2SnC after oxidation via open-air furnacing (A) and rapid thermal annealing (B). The black tie-line represents anatase TiO_2 (RRUFF R070582), the blue represents rutile TiO_2 (RRUFF R050031), and the pink represents SnO_2 (RRUFF R050502). The black diamond and black circle indicate the D- and G-bands of carbon, respectively.

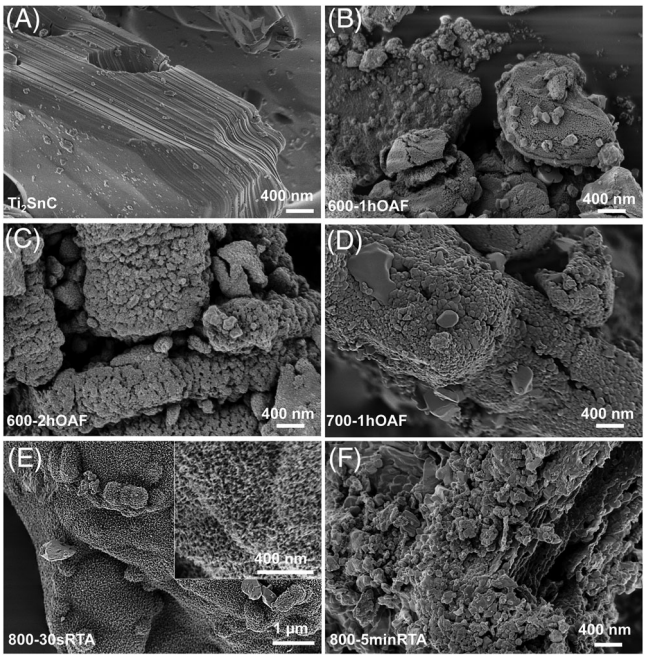

FIGURE 4 Scanning electron micrographs of the pristine Ti_2SnC (A) and oxidized samples 600-1hOAF (B), 600-2hOAF (C), 700-1hOAF (D), 800-30sRTA with inset showing a higher magnification of the same sample (E), 800-5minRTA (F).

the samples treated at lower temperatures present broader bands characteristic of amorphized species. The increase in temperature and holding time led to a higher graphitization degree with a well-defined G-band in the 700-1hOAF sample. However, due to high temperature and oxidizing conditions, further oxidation with prolonged time led to the complete removal of carbon species in 700-2hOAF. The RTA samples also feature a carbon signal, and carbon is retained in all samples for temperatures of 700°C and above.

Another set of spectral changes occurs in the region below 900 cm^{-1}. The pristine MAX phase shows bands at 247 and 347 cm^{-1} corresponding to the E_{1g} and A_{1g} modes, respectively.[42] After the thermal treatments, these bands are replaced by characteristic oxide signals. Rutile TiO_2 shows distinctive bands at 440 cm^{-1} (E_g) and 610 cm^{-1} (A_{1g}), besides a broad band at ca. 235 cm^{-1} assigned to the disordered-induced multi-phonon process.[43] Meanwhile, SnO_2 is characterized by a low-intensity band at about 560 cm^{-1}, an intense band at 630 cm^{-1} (A_{1g} mode), and a broader signal at about 770 cm^{-1} (B_2).[44] Most spectra show a characteristic profile of the TiO_2 rutile phase, especially for the treatments at higher temperatures/holding times. For the RTA samples at reduced treatment times, there is band broadening or the emergence of a shoulder corresponding to the presence of SnO_2 in the sample. Several works observed similar behaviors where mixtures of TiO_2 and SnO_2 with Ti content as little as 9 mass% led to a complete eclipse of SnO_2 bands.[45–47]

For further characterization and electrochemical investigations, we chose the following samples: 600-1h-OAF, 600-2hOAF, 700-1hOAF, 800-30sRTA, and 800-5minRTA. These samples possessed the desired composition of SnO_2, TiO_2, and residual MAX carbide, with approximate total oxide weight percentages of at least 50% and Ti_2SnC weight percentages below 30% (excluding 700-1hOAF, which indicated no Ti_2SnC presence) according to the Rietveld fit analysis of XRD patterns (Figures S2 and S3).

In the next step, we investigated the morphology of the oxidized samples by SEM (Figure 4). The SEMs reveal oxidized particles coating the tops and edges of the layered MAX sheets in the range of 0.2–2 μm. These oxide particles are crystalline (with the size of <200 nm) and much smaller than the MAX phase particle size, allowing for a relatively uniform coating of the MAX layers. As expected, 700-1hOAF had no layered morphology, displaying only oxide particles supporting the absence of Ti_2SnC in Rietveld analysis and XRD. Raman spectroscopy also indicates the presence of amorphous carbon. 800-30sRTA showed the most uniform coating of oxide particles among the samples.

The nanostructure of the hybrid material is seen more clearly at higher resolution using TEM. We exemplify this by choosing 800-30sRTA. It showed the most promising microstructure using SEM (Figure 4E), a complex composition indicated by XRD, and (as shown in a later section) provided attractive electrochemical performance. TEMs (Figure 5) of 800-30sRTA show sheetlike particles composed of smaller particles agglomerates, which constitute most of the sample. The smaller particles present crystalline domains below 20 nm and are homogeneously distributed in an incompletely crystalline. The lattice fringe spacings in these domains correspond to the

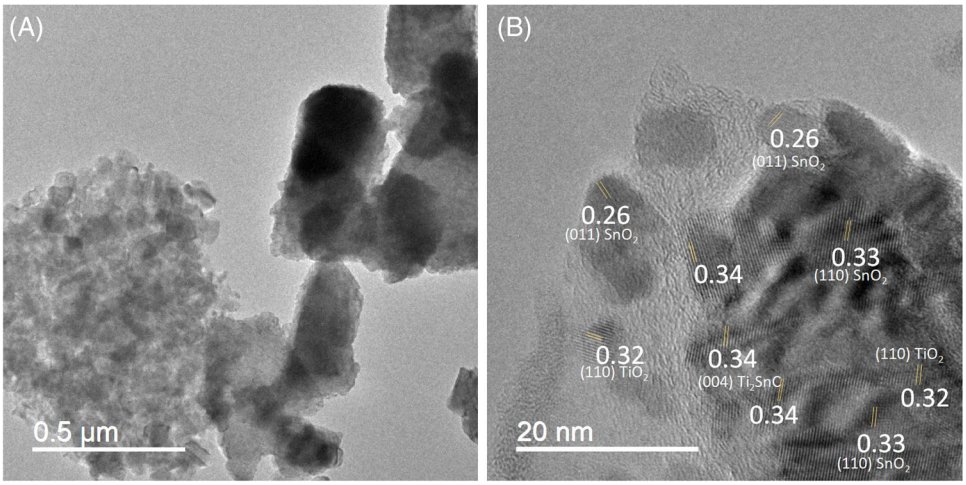

FIGURE 5 Transmission electron micrographs of the 800-30sRTA sample (A) overview at low magnifiifcation, and (B) with details of the crystallite fringes and corresponding phases.

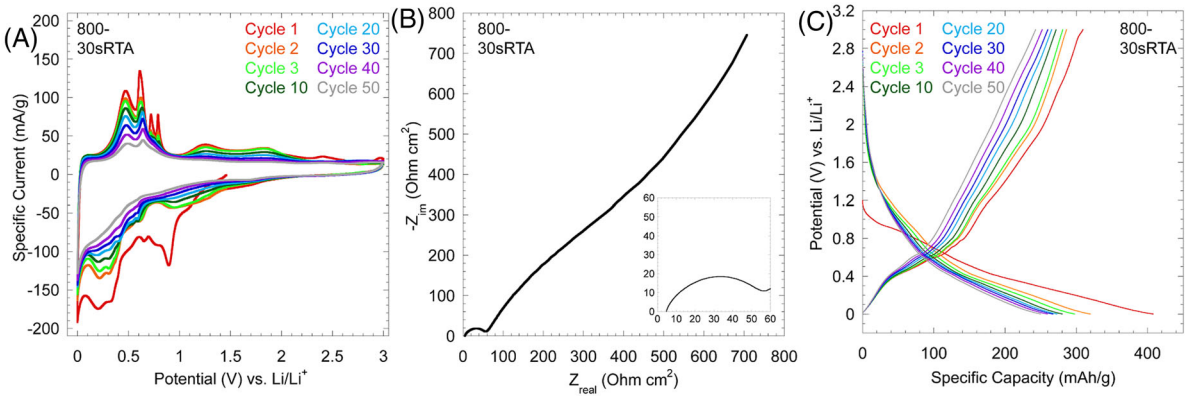

FIGURE 6 Electrochemical data for 800-30sRTA: cyclic voltammograms recorded at 0.1 mV/s over 50 cycles (A), electrochemical impedance spectrum (B), and galvanostatic charge/discharge voltage profile at 100 mA/g (C).

d-spacing of 3.24 Å for (110) of rutile (PDF 01-1291), 3.40 Å for (110), and 2.67 Å for (101) of SnO_2 (PDF 01-0625), and 2.91 Å for (200) of tin (PDF 01-0926).

3.2 | Electrochemical performance

Our study aims to establish the electrochemical performance of oxidized Ti_2SnC hybrid materials as lithium-ion battery electrodes. To this end, we conducted a series of electrochemical benchmarking experiments in alignment with the state-of-the-art. To study the electrochemical performance of this anode material, cyclic voltammetry between 0.001 and 3.0 V versus Li/Li^+ at 0.1 mV/s and EIS were performed (Figure 6 and Figures S4–S7). Cyclic voltammetry over 50 cycles (Figure 6A) indicates the primary reversible oxidation peaks between 0.4 and 0.7 V versus Li/Li^+ and two secondary sharp oxidation peaks between 0.70 and 0.85 V versus Li/Li^+. Furthermore, there is a secondary reduction peak around 0.9 versus Li/Li^+. These secondary peaks can be attributed to reactions alongside the primary oxidation and reduction typical to SnO_2.[48,49] The phases responsible for these reactions are consumed over time. Thus, the peaks are no longer present beyond the 10th cycle. A reduction in the redox peaks' intensity over cycling was also observed in the other oxidized samples (Figures S4–S7), with various heating times, indicating no relative change of side reactions between shorter and longer heating times.

Previous work has demonstrated that SnO_2 has a single primary oxidation peak around 0.75 V, a broad secondary oxidation peak around 1.3 V, and a secondary reduction peak around 0.80 V.[49] Similarly, SnO_2 shows two primary oxidation peaks between 0.50 and 0.65 V, two secondary oxidation peaks between 0.70 and 0.80 V, and a secondary reduction peak at 0.90 V.[50] Rutile-type TiO_2 typically presents oxidation and reduction peaks between 2.6 and 1.0 V with very broad redox processes, leading

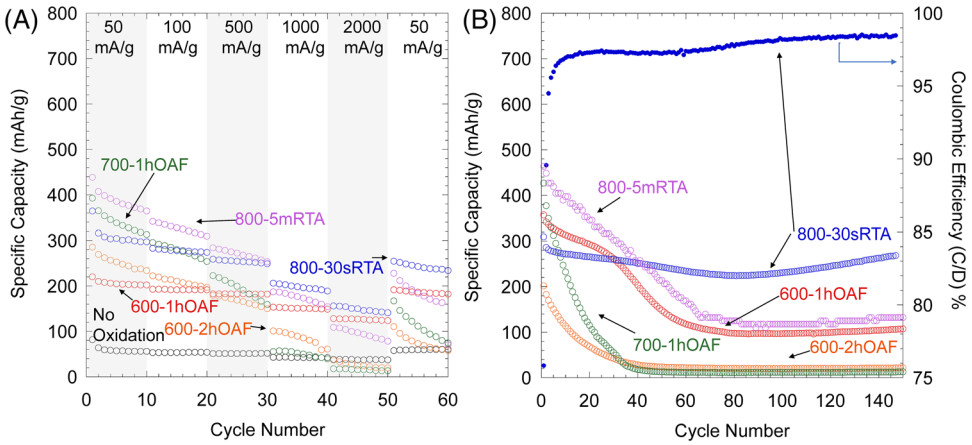

FIGURE 7 Specific charge capacity per cycle at specific currents of 50, 100, 200, 500, 1000, 2000, and 50 mA/g for open-air furnace (OAF) and rapid thermal annealing (RTA) samples (A). Specific capacity (outline dots) and Coulombic efficiency (solid dots) per cycle for a constant current of 100 mA/g over 100 cycles for OAF and RTA samples (B).

to a continuous charge/discharge slope with no defined plateaus.[51,52]

The electrochemical impedance spectra (Figure 6B) show a system resistance of approximately 4.1 Ω and a semicircle showing a charge transfer resistance of approximately 46.1 Ω. Of the other investigated samples, 600-1hOAF and 600-2hOAF, show a higher system resistance but comparable charge transfer resistance (Figures S4B–S5B), 700-1hOAF shows a comparable system resistance, but a larger charge transfer resistance (Figure S6B), and 800-5mRTA shows higher charge transfer resistance of ca. 117 Ω (Figure S7). A direct comparison of 800-30sRTA to 800-5mRTA and 600-1hOAF is shown in Figure S8 as well as the circuit fitting parameters in Table S1. Besides the presence of TiC and more Ti_2SnC, this sample also presents a smaller content of TiO_2, which could lead to better charge transport within the sample, as is observed that small amounts of TiO_2 in SnO_2 samples can decrease its bandgap.[53]

In the next step, we investigated the electrochemical charge/discharge behavior at varying rates. To study the rate handling capability, the assembled coin cells were electrochemically cycled between 1 mV and 3 V versus Li/Li^+ at specific currents of 50, 100, 200, 1000, 2000, and 50 mA/g to observe the specific capacity and cycling stability of the electrodes (Figure 7A and Figure S9A). At initial low rates of 50 mA/g, capacity values ranged from about 200 mAh/g (600-1hOAF) to approximately 400 mAh/g (800-5minRTA). At very high rates of 2000 mA/g, among all tested samples, the 800-30sRTA sample exhibited the highest capacity of 150 mAh/g. This excellent rate handling capability for the 800-30sRTA sample can be attributed to its mixed composition, where residual Ti_2SnC alongside TiC and metallic Sn and carbon byproducts provide high electrical conductivity.

The coin cells were further investigated at a constant current density of 100 mA/g to determine the longevity and stability of the anodes (Figure 7B). Initial lithiation and delithiation capacities for 600-1hOAF were 502 and 357 mAh/g, respectively, whereas they were 383 and 202 mAh/g for 600°C at 2 h, and 838 and 427 mAh/g for 700°C at 1 h, but these values dropped to values below 100 mAh/g after 100 cycles. Electrodes from 800-5minRTA displayed an initial lithiation capacity of 735 mAh/g and a delithiation capacity of 463 mAh/g, both of which degraded substantially over 100 cycles. However, RTA 800-30sRTA displayed initial lithiation and delithiation capacities of 408 and 309 mAh/g, which only reduced to a reversible capacity of around 230 mAh/g after 100 cycles that increased then to around 270 mAh/g after 150 cycles.

The values of Coulombic efficiency remain at around 97% until approximately 60 cycles. It increases to 98.5% after 150 cycles, confirming the expected decrease in lost Li^+ with increased cycling. The initial Coulombic efficiency displayed by this material is low. This may align with lithium consumption from irreversible side reactions caused by the synthesis procedure, which could likely be eliminated with further optimization of the synthesis methodology. For clarity, the Coulombic efficiency values of the remaining stability curves are presented in Figure S9B.

Direct comparison between the same temperature conditions indicates that the samples with longer holding times exhibit higher specific capacities. Still, these values degrade more rapidly than in their lower-holding time counterparts. We attribute this increased initial value and quick degradation to the higher ratio of metal oxides to unoxidized Ti_2SnC in the longer heating time samples, as SnO_2 has a high theoretical capacity (782 mAh/g),[48] but it displays capacity degradation due to the stress of

lithium insertion.[19–21] This trend is even more intense between samples of two oxidation temperatures with the same holding time, meaning that the higher temperature is associated with a lower relative concentration of Ti_2SnC. For example, Ti_2SnC content dropped from ≈28 mass% in 600-1hOAF to ≈0% in 700-1hOAF, and this drop is accompanied by a drop of cyclability as the specific capacity faded less than 20 mAh/g after 40 cycles for 700-1hOAF, whereas it was still around 206 mAh/g for 600-1hOAF despite the higher initial specific capacity of 700-1hOAF (838 mAh/g) than that of 600-1hOAF (503 mAh/g).

Although a further investigation into the specific mechanisms of lithium storage present in these composites is necessary, previous literature provides an understanding of the likely pathways. The low experimental capacities of Sn-containing MAX phases align with nonsignificant changes in the morphology and structure of the ceramic material.[33,34] It is well established that the electroactivity of TiO_2 comes from the intercalation and deintercalation of lithium. However, this diffusion-limited process can vary among forms of TiO_2.[12,14,15,17] SnO_2 also undergoes an alloying reaction with lithium, causing the volume expansion issues associated with pure SnO_2 anodes.[18,19] As the pure Ti_2SnC samples demonstrated very low capacities, our composite materials exhibit lithiation via Li-ion intercalation into TiO_2 and an alloying reaction with SnO_2.

These capacity results align with previous work on tin and titanium oxide anodes, which typically demonstrate capacity values between 150 and 250 mAh/g for TiO_2 (Refs. [7, 9–12, 16, 17, 54, 55]) and 400 and 800 mAh/g for SnO_2 (Refs. [20, 56–58]). Materials like SnO_2-modified TiO_2 have demonstrated initial capacity values between 350 and 450 mAh/g at 100 mA/g,[55] which is very well aligned with the results of this study. However, M_2SnX phases have demonstrated capacities below the theoretical capacity of Sn, with Nb_2SnC showing capacities below 200 mA/g when used as an anode for LIBs.[33,34] Currently, most commercially available anodes are made of graphite, with a theoretical capacity of 372 mAh/g.[59] Although this value is still marginally higher than the experimentally observed capacity of 800-30sRTA, likely, further development of the structure and composition of this composite material could easily allow the outperformance of graphite. Based on these results, 800-30sRTA shows a preferable composition of carbide and oxides for an anode material, as it displays the best combination of high capacity and stability over time.

4 | CONCLUSIONS

Thermal oxidation of Ti_2SnC in air using slow and rapid heating conditions resulted in the TiO_2–SnO_x–Ti_2SnC/TiC/C hybrid materials, as confirmed and characterized by XRD, Raman spectroscopy, and electron microscopy. The structure, composition, and respective phase content within these hybrid materials strongly depend on the oxidation conditions. Lower temperatures allowed for slow direct oxidation of Ti_2SnC to form a coating of small TiO_2 and SnO_2 particles, whereas higher temperatures and limited oxygen supply facilitated a rapid decomposition of Ti_2SnC to also form TiC and bound metallic Sn. Combining conductive materials (carbide/carbon) and electrochemically active metal oxides (namely, titania and tin oxide) makes the hybrid materials highly attractive for use as LIB anodes.

Among the tested samples, 800-5minRTA (consisted of mainly TiO_2–SnO_x–C with about 15 mass% TiC and <2 mass% Ti_2SnC) achieved 735 mAh/g capacity at 100 mA/g, but it was not stable as the capacity faded to 117 mAh/g after 100 cycles. RTA of Ti_2SnC in air at 800°C for 30 s that exhibited more Ti_2SnC (≈10 mass%) than 800-5minRTA produced the electrochemically most efficient composition of carbides and oxides for LIBs as it displayed a stable reversible capacity of around 270 mAh/g after 150 cycles. This sample also showed an excellent capability to handle a high cycling rate; demonstrating a specific capacity of 150 mAh/g at 2000 mA/g. The higher Ti_2SnC content enhanced the electrical conductivity and mechanical stability of the hybrid. Although further investigation will have to address this material's specific morphology and longevity, our data demonstrate the viability of using one single-MAX phase (namely, Ti_2SnC) as a precursor for mixed oxides/carbide/carbon hybrid materials. This technique results in improved electrochemical performance over the as-synthesized MAX phase, which is limited to surface lithium interaction, opening the material family up for further energy storage applications. Considering that carbide MAX phases containing V, Cr, Nb, Mo, Hf, Ga, In, and Sn can be produced, realizing hybrid structures of these metal oxides with carbon and carbides will be of interest for many applications varying from energy storage to catalysis, electronics, and sensing.

ACKNOWLEDGMENTS

Materials synthesis and electrochemical testing done at Tulane University were supported as part of the Fluid Interface Reactions, Structures, and Transport (FIRST) Center, an Energy Frontier Research Center (EFRC) funded by the United States Department of Energy (DOE), Office of Science, Office of Basic Energy Sciences. The INM authors thank Eduard Arzt (INM) for his continuing support. VP and SH acknowledge funding of the electroMOXene project (PR-1173/9) by the German Research Foundation (DFG, Deutsche Forschungsgemeinschaft).

Open access funding enabled and organized by Projekt DEAL.

ORCID

Samantha Husmann https://orcid.org/0000-0001-6157-214X
Volker Presser https://orcid.org/0000-0003-2181-0590
Michael Naguib https://orcid.org/0000-0002-4952-9023

REFERENCES

1. Dunn B, Kamath H, Tarascon JM. Electrical energy storage for the grid: a battery of choices. Science. 2011;334(6058):928–35.
2. Wang L. Synthesis, characterizations, and utilization of oxygen-deficient metal oxides for lithium/sodium-ion batteries and supercapacitors. Coord Chem Rev. 2019;397:138–68.
3. Liao J, Tan R, Kuang Z, Cui C, Wei Z, Deng X, et al. Controlling the morphology, size and phase of Nb_2O_5 crystals for high electrochemical performance. Chin Chem Lett. 2018;29(12):1785–90.
4. Gogotsi Y. What nano can do for energy storage? ACS Nano. 2014;8(6):5369–71.
5. Lamberti A, Garino N, Sacco A, Bianco S, Chiodoni A, Gerbaldi C. As-grown vertically aligned amorphous TiO_2 nanotube arrays as high-rate Li-based micro-battery anodes with improved long-term performance. Electrochim Acta. 2015;151:222–9.
6. Huang SY, Kavan L, Exnar I, Grätzel M. Rocking chair lithium battery based on nanocrystalline TiO_2 (anatase). J Electrochem Soc. 1995;142(9):L142–4.
7. Kim C, Buonsanti R, Yaylian R, Milliron DJ, Cabana J. Carbon-free TiO_2 battery electrodes enabled by morphological control at the nanoscale. Adv Energy Mater. 2013;3(10):1286–91.
8. Fehse M, Ventosa E. Is TiO_2(B) the future of titanium-based battery materials? ChemPlusChem. 2015;80(5):785–95.
9. Madian M, Eychmüller A, Giebeler L. Current advances in TiO_2-based nanostructure electrodes for high performance lithium ion batteries. Batteries. 2018;4(1):7.
10. Wei W, Ihrfors C, Björefors F, Nyholm L. Capacity limiting effects for freestanding, monolithic TiO_2 nanotube electrodes with high mass loadings. ACS Appl Energy Mater. 2020;3(5):4638–49.
11. Jiang C, Zhang J. Nanoengineering titania for high rate lithium storage: a review. J Mater Sci Technol. 2013;29(2):97–122.
12. Nuspl G, Yoshizawa K, Yamabe T. Lithium intercalation in TiO_2 modifications. J Mater Chem. 1997;7(12):2529–36.
13. Kavan L. Lithium insertion into TiO_2 (anatase): electrochemistry, Raman spectroscopy, and isotope labeling. J Solid State Electrochem. 2014;18(8):2297–306.
14. Koudriachova M. Diffusion of Li-ions in rutile. An ab initio study. Solid State Ionics. 2003;157(1–4):35–8.
15. Van De Krol R, Goossens A, Schoonman J. Spatial extent of lithium intercalation in anatase TiO_2. J Phys Chem B. 1999;103(34):7151–9.
16. Liu Y, Yang Y. Recent progress of TiO_2-based anodes for Li ion batteries. J Nanomater. 2016;2016:8123652.
17. Liu Z, Andreev YG, Robert Armstrong A, Brutti S, Ren Y, Bruce PG. Nanostructured TiO_2(B): the effect of size and shape on anode properties for Li-ion batteries. Prog Nat Sci: Mater Int. 2013;23(3):235–44.
18. Yang J. Small particle size multiphase Li-alloy anodes for lithium-ion-batteries. Solid State Ionics. 1996;90(1–4):281–7.
19. Courtney IA, Dahn JR. Electrochemical and in situ X-ray diffraction studies of the reaction of lithium with tin oxide composites. J Electrochem Soc. 1997;144(6):2045–52.
20. Sui X, Huang X, Wu Y, Ren R, Pu H, Chang J, et al. Organometallic precursor-derived SnO_2/Sn-reduced graphene oxide sandwiched nanocomposite anode with superior lithium storage capacity. ACS Appl Mater Interfaces. 2018;10(31):26170–7.
21. Li X, Dhanabalan A, Gu L, Wang C. Three-dimensional porous core-shell Sn@carbon composite anodes for high-performance lithium-ion battery applications. Adv Energy Mater. 2012;2(2):238–44.
22. Wang X, Zhou X, Yao K, Zhang J, Liu Z. A SnO_2/graphene composite as a high stability electrode for lithium ion batteries. Carbon. 2011;49(1):133–9.
23. Yao J, Shen X, Wang B, Liu H, Wang G. In situ chemical synthesis of SnO_2-graphene nanocomposite as anode materials for lithium-ion batteries. Electrochem Commun. 2009;11(10):1849–52.
24. Wang D, Choi D, Li J, Yang Z, Nie Z, Kou R, et al. Self-assembled TiO_2-graphene hybrid nanostructures for enhanced Li-ion insertion. ACS Nano. 2009;3(4):907–14.
25. Qiu B, Xing M, Zhang J. Mesoporous TiO_2 nanocrystals grown in situ on graphene aerogels for high photocatalysis and lithium-ion batteries. J Am Chem Soc. 2014;136(16):5852–5.
26. Sokol M, Natu V, Kota S, Barsoum MW. On the chemical diversity of the MAX phases. Trends Chem. 2019;1(2):210–23.
27. Gogotsi Y, Anasori B. The rise of MXenes. ACS Nano. 2019;13(8):8491–4.
28. Tang Q, Zhou Z, Shen P. Are MXenes promising anode materials for Li ion batteries? Computational studies on electronic properties and Li storage capability of Ti_3C_2 and $Ti_3C_2X_2$ (X = F, OH) Monolayer. J Am Chem Soc. 2012;134(40):16909–16.
29. Barsoum MW, Radovic M. Elastic and mechanical properties of the MAX phases. Annu Rev Mater Res. 2011;41(1):195–227.
30. Naguib M, Come J, Dyatkin B, Presser V, Taberna P-L, Simon P, et al. MXene: a promising transition metal carbide anode for lithium-ion batteries. Electrochem Commun. 2012;16(1):61–4.
31. Naguib M, Mashtalir O, Lukatskaya MR, Dyatkin B, Zhang C, Presser V, et al. One-step synthesis of nanocrystalline transition metal oxides on thin sheets of disordered graphitic carbon by oxidation of MXenes. Chem Commun. 2014;50(56):7420–3.
32. Zhao M-Q, Torelli M, Ren CE, Ghidiu M, Ling Z, Anasori B, et al. 2D titanium carbide and transition metal oxides hybrid electrodes for Li-ion storage. Nano Energy. 2016;30:603–13.
33. Zhao S, Dall'Agnese Y, Chu X, Zhao X, Gogotsi Y, Gao Y. Electrochemical interaction of Sn-containing MAX phase (Nb_2SnC) with Li-Ions. ACS Energy Lett. 2019;4(10):2452–7.
34. Li Y, Ma G, Shao H, Xiao P, Lu J, Xu J, et al. Electrochemical lithium storage performance of molten salt derived V_2SnC MAX phase. Nano-Micro Lett. 2021;13(1):158.
35. Tesfaye AT, Mashtalir O, Naguib M, Barsoum MW, Gogotsi Y, Djenizian T. Anodized Ti_3SiC_2 As an anode material for Li-ion microbatteries. ACS Appl Mater Interfaces. 2016;8(26):16670–6.
36. Husmann S, Besch M, Ying B, Tabassum A, Naguib M, Presser V. Layered titanium niobium oxides derived from solid-solution Ti–Nb carbides (MXene) as anode materials for Li-ion batteries. ACS Appl Energy Mater. 2022;5(7):8132–42.

37. Budak Ö, Geißler M, Becker D, Kruth A, Quade A, Haberkorn R, et al. Carbide-derived niobium pentoxide with enhanced charge storage capacity for use as a lithium-ion battery electrode. ACS Appl Energy Mater. 2020;3(5):4275–85.
38. Zhou YC, Dong HY, Wang XH. High-temperature oxidation behavior of a polycrystalline Ti_2SnC ceramic. Oxid Met. 2004;61(5/6):365–77.
39. Bei G, Pedimonte BJ, Fey T, Greil P. Oxidation behavior of MAX phase $Ti_2Al_{(1-x)}Sn_xC$ solid solution. J Am Ceram Soc. 2013;96(5):1359–62.
40. Dong HY, Yan CK, Chen SQ, Zhou YC. Solid-liquid reaction synthesis and thermal stability of Ti_2SnC powders. J Mater Chem. 2001;11(5):1402–7.
41. Zhang J, Liu B, Wang JY, Zhou YC. Low-temperature instability of Ti_2SnC: a combined transmission electron microscopy, differential scanning calorimetry, and x-ray diffraction investigations. J Mater Res. 2012;24(1):39–49.
42. Bentzel GW, Naguib M, Lane NJ, Vogel SC, Presser V, Dubois S, et al. High-temperature neutron diffraction, Raman spectroscopy, and first-principles calculations of Ti_3SnC_2 and Ti_2SnC. J Am Ceram Soc. 2016;99(7):2233–42.
43. Ma HL, Yang JY, Dai Y, Zhang YB, Lu B, Ma GH. Raman study of phase transformation of TiO_2 rutile single crystal irradiated by infrared femtosecond laser. Appl Surf Sci. 2007;253(18):7497–500.
44. Zuo J, Xu C, Liu X, Wang C, Wang C, Hu Y, et al. Study of the Raman spectrum of nanometer SnO_2. J Appl Phys. 1994;75(3):1835–6.
45. Tricoli A, Righettoni M, Pratsinis SE. Minimal cross-sensitivity to humidity during ethanol detection by SnO_2-TiO_2 solid solutions. Nanotechnology. 2009;20(31):315502.
46. Liu S, Li Y, Xie M, Guo X, Ji W, Ding W. One-pot synthesis of intestine-like SnO_2/TiO_2 hollow nanostructures. Mater Lett. 2010;64(3):402–4.
47. Hirata T, Ishioka K, Kitajima M, Doi H. Concentration dependence of optical phonons in the TiO_2-SnO_2 system. Phys Rev B. 1996;53(13):8442.
48. Wang Y, Huang ZX, Shi Y, Wong JI, Ding M, Yang HY. Designed hybrid nanostructure with catalytic effect: beyond the theoretical capacity of SnO_2 anode material for lithium ion batteries. Sci Rep. 2015;5(1):9164.
49. Ding L, He S, Miao S, Jorgensen MR, Leubner S, Yan C, et al. Ultrasmall SnO_2 nanocrystals: hot-bubbling synthesis, encapsulation in carbon layers and applications in high capacity Li-ion storage. Sci Rep. 2014;4(1):4647.
50. Shin JH, Song JY. Electrochemical properties of Sn-decorated SnO nanobranches as an anode of Li-ion battery. Nano Converg. 2016;3(1):9.
51. Cherian CT, Reddy M, Magdaleno T, Sow C-H, Ramanujachary K, Rao GS, et al. (N, F)-Co-doped TiO_2: synthesis, anatase-rutile conversion and Li-cycling properties. CrystEngComm. 2012;14(3):978–86.
52. Zhang Y, Pu X, Yang Y, Zhu Y, Hou H, Jing M, et al. An electrochemical investigation of rutile TiO_2 microspheres anchored by nanoneedle clusters for sodium storage. Phys Chem Chem Phys. 2015;17(24):15764–70.
53. Zakrzewska K. Mixed oxides as gas sensors. Thin Solid Films. 2001;391(2):229–38.
54. Patil SB, Phattepur H, Kishore B, Viswanatha R, Nagaraju G. Robust electrochemistry of black TiO_2 as stable and high-rate negative electrode for lithium-ion batteries. Mater Renew Sustain Energy. 2019;8(2):10.
55. Lübke M, Johnson I, Makwana NM, Brett D, Shearing P, Liu Z, et al. High power TiO_2 and high capacity Sn-doped TiO_2 nanomaterial anodes for lithium-ion batteries. J Power Sources. 2015;294:94–102.
56. Dai L, Zhong X, Zou J, Fu B, Su Y, Ren C, et al. Highly Ordered SnO_2 nanopillar array as binder-free anodes for long-life and high-rate Li-ion batteries. Nanomaterials. 2021;11(5):1307.
57. Dixon D, Ávila M, Ehrenberg H, Bhaskar A. Difference in electrochemical mechanism of SnO_2 conversion in lithium-ion and sodium-ion batteries: combined in operando and ex situ XAS investigations. ACS Omega. 2019;4(6):9731–8.
58. Faramarzi MS, Abnavi A, Ghasemi S, Sanaee Z. Nanoribbons of SnO_2 as a high performance Li-ion battery anode material. Mater Res Express. 2018;5(6):065040.
59. Zhang H, Yang Y, Ren D, Wang L, He X. Graphite as anode materials: fundamental mechanism, recent progress and advances. Energy Storage Mater. 2021;36:147–70.

SUPPORTING INFORMATION

Additional supporting information can be found online in the Supporting Information section at the end of this article.

How to cite this article: Jolly S, Husmann S, Presser V, Naguib M. Growth of titania and tin oxide from Ti_2SnC via rapid thermal oxidation in air for lithium-ion battery application. J Am Ceram Soc. 2023;106:3261–3271.
https://doi.org/10.1111/jace.19010